Force-chain distributions in granular systems

Ling Zhang,[1] Yujie Wang,[1] and Jie Zhang[1,2,*]

[1]*Department of Physics and Astronomy, Shanghai Jiao Tong University, Shanghai 200240, China*

[2]*Institute of Natural Sciences, Shanghai Jiao Tong University, Shanghai 200240, China*

(Received 27 January 2013; revised manuscript received 31 October 2013; published 21 January 2014)

We study experimentally the distributions of force chains in granular materials, which are slightly different in sheared systems compared to isotropically compressed systems, especially at the tails, reflecting the shear-induced anisotropy of the contact force network. Ignoring this anisotropy allows us to establish a relationship between the mean force-chain length L_m and the average contact number Z of particles for both systems, independent of the system size. We also demonstrate that force-chain distributions are not related to the exponential-like distributions of stresses.

DOI: 10.1103/PhysRevE.89.012203 PACS number(s): 45.70.−n, 61.43.−j, 81.05.Rm, 83.80.Fg

I. INTRODUCTION

In granular materials, although each particle can be well characterized individually, describing an assembly of densely packed grains interacting only via contacts remains a significant challenge because (1) thermal energy is negligible and (2) observed fluctuations are often large [1,2]. One striking example is the presence of "force chains" in the way external forces are distributed through filament-like clusters of particles. Force chains are observed in three-dimensional (3D) systems [3] as well as in two-dimensional (2D) systems using *photoelastic* techniques [4–6]. The study of force chains is crucial in understanding various properties of granular materials. These include the jamming of fragile matter [7,8], the emergence of shear jammed states [9], an abrupt termination of flow in a hopper [10], the bimodal characteristics of the stress transmission [11], point force responses of granular systems [5,6], the Janssen effect [12], sound propagations in granular packings [13,14], and snow avalanches and earthquakes [15].

Despite the great importance, direct measurements of force chains are rare [16,17]. Instead, extensive studies have been focused on the distributions of contact forces [3,6,18–22] and on the structures of packings [23–25] in the past decade.

Here we report a precise experimental measurement of force chains in two model systems: pure shear and isotropic compression. We establish firmly that the statistics of force-chain distributions is very rich. Applying shear creates anisotropy in force-chain networks and thus changes the force-chain length distributions. Despite the broad distributions, the mean length scale of the force chains L_m is understood as a function of the average contact number per particle, Z. L_m first increases rapidly and then reaches a plateau as the system size increases; in the present system, L_m is already in the thermal dynamic limit. Using a mean-field model, we can predict such a relationship quantitatively, with a reasonable agreement with the experimental measurements. In addition, we demonstrate that the stress distributions and force-chain length distributions are two separate problems. For each individual result, we find that it is robust and consistent within a range of parameter values in the force-chain identification algorithm.

II. EXPERIMENTAL METHODS

In this study, we analyze data obtained from two different experiments using a biaxial apparatus [9,26]. Briefly, a "biax" consists of a rectangular frame, within which a total of 1568 disks are randomly deposited on a powder-lubricated Plexiglas surface, with roughly 80% small disks of a diameter of 0.74 cm and 20% large disks of a diameter of 0.86 cm. Starting from a square, isotropic compression is achieved by gradually reducing the original square to a series of smaller squares until a final packing fraction Φ is reached. In isotropic compression, the data were obtained at $\Phi = 0.842$ and $\Phi = 0.848$, respectively. In contrast, pure shear is applied by compressing one pair of parallel boundaries and expanding the other pair while keeping the area of the rectangle fixed. In pure shear, data were obtained at $\Phi = 0.828$ and at strains of 2% and 3%, respectively, where shear-jammed states were developed [9]. In a given experiment, multiple runs, up to a few hundred, were performed under the same conditions to create an ensemble. Each run is called a realization with multiple images of the photoelastic disks taken, including one (respectively, the other) in the absence of (respectively, in the presence of) a pair of circular polarizer sheets [26].

Applying an image processing and a force-inverse algorithm allows us to determine the radius and the position of each particle, the interparticle contacts, and the vector contact forces between particles with reasonable precision [6,9,26]. The force-moment tensor of a particle is defined as $\widehat{\sigma_{ij}} = \sum_k f_{ik} R_{jk}$. Here f_{ik} is the ith component of the contact force at the kth contact of the particle and R_{jk} is the jth component of its branching vector pointing from its center to its kth contact. The summation is over all contacts of the particle.

To analyze the force-chain statistics, one must first define a force chain. We use a force-chain definition similar to that of Ref. [16]. First, among all force-bearing particles, only those with $\sigma_1 \geqslant \langle\sigma_1\rangle$ are selected, where σ_1 is the maximum absolute eigenvalue of $\widehat{\sigma_{ij}}$ and $\langle\rangle$ averages over different particles in a single realization. Second, each force-bearing particle carries a unique orientation specified by the + or − directions of the eigenvector of σ_1, which shall align for particles of the same force chain. A threshold angle δ is introduced to quantify the alignment. Figure 1(a) shows a schematic of two perfectly aligned force chains, $O_1O_2O_3$ and

*jiezhang2012@sjtu.edu.cn

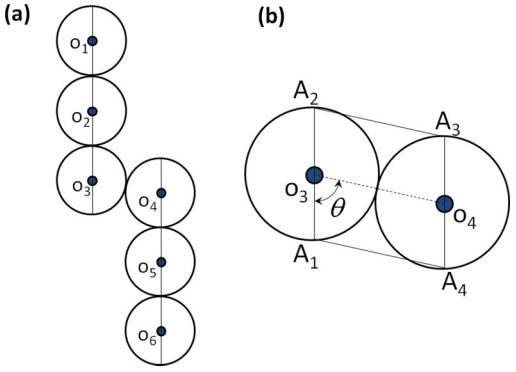

FIG. 1. (Color online) (a), (b) Schematic that illustrates the necessity of introducing a coefficient α, or equivalently a threshold angle θ, in order to distinguish two ideally straight force chains, i.e., chains $O_1O_2O_3$ and $O_4O_5O_6$. The angle θ is defined as the angle between the orientation of the local force moment tensor of disk O_3 and the center-to-center line O_3O_4.

$O_4O_5O_6$. In order to differentiate these two force chains, the third criterion is introduced to compare the directions of A_1A_2 and A_3A_4 of the particles O_3 and O_4 with the line O_3O_4. The actual algorithm is implemented by comparing the area of the polygon $A_1A_2A_3A_4$ to the sum of the areas of the two disks multiplied by a coefficient α, as drawn in Fig. 1(b). An $\alpha = 0.25$ is equivalent to $\theta = 23^\circ$ for two perfectly aligned particles O_3 and O_4. We note that twice θ is 46°, consistent with the 45° threshold angle used in Ref. [16]. We further note that twice δ is 40° for $\alpha = 0$, i.e., $\theta = 0$ in Fig. 1, which is also consistent with the 45° threshold angle used in Ref. [16]. We will present results below first for $\delta = 20^\circ$ and $\alpha = 0.25$, and more detailed studies of δ and α at other values will then be presented afterwards. Compared with Ref. [16], there are two major differences: First, in our definition, the shortest force chain consists of two particles instead of three. Second, our method considers the branching of force chains, i.e., only the best aligned neighboring particle is selected. One sample image of the detected force chains is plotted in Fig. 2 for $\alpha = 0.25$ and $\delta = 20^\circ$.

III. RESULTS AND DISCUSSION

Figure 3 main panels show two typical distributions of force-chain lengths using open circles for pure shear (a) and isotropic compression (b) at $\alpha = 0.25$ and $\delta = 20^\circ$. To get better statistics, the results in Fig. 3(a) [respectively, in Fig. 3(b)] are produced from a subensemble of 103 (respectively, 67) realizations at $Z = 3.93 \pm 0.04$ (respectively, at $Z = 4.22 \pm 0.04$). Except at the tail part, the distribution can be fit well using an exponential function $P(N) \propto e^{-N/\lambda}$ of one free parameter: for pure shear, it shows a deviation from the exponential fit, with a fat tail better fit using a stretched exponential function $P(N) \propto e^{-[(N-2)/\Delta]^\beta}$ of two free parameters Δ and β. At $\alpha = 0.25$ and $\delta = 20^\circ$, the fitting parameters λ, Δ, and β are respectively 1.36, 1.27, and 0.84 in Fig. 3(a) and 0.98, 0.95, and 0.93 in Fig. 3(b). We conjecture that for an ideal isotropic compression with a zero shear stress $\beta = 1.0$, recovering an exponential distribution. We believe that the slight deviation was because of the existence of a

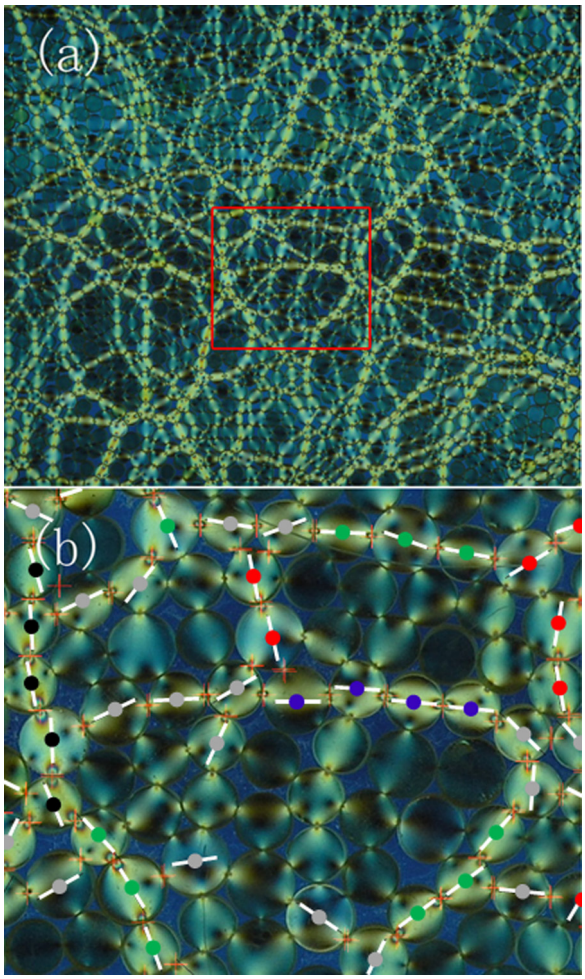

FIG. 2. (Color online) (a) An example of a force-chain network in a 2D layer of granular materials under isotropic compression. Here bidisperse photoelastic disks are used. (b) The portion of panel (a) indicated by the red rectangle, showing several force chains of different lengths using different colors. For example, chains of different lengths are displayed by painting each particle center using dots of different colors: black for length five, blue for length four, green for length three, and red for length two. The short line drawn on top of each particle represents the orientation of the force moment tensor of each particle. Particles with gray-dot centers do not belong to any force chain although satisfying $\sigma_1 \geqslant \langle\sigma_1\rangle$ (see Sec. II for details).

nonzero, albeit small, shear stress in the system. In contrast, once the shear is applied, creating anisotropy of the force-chain network [6], the force-chain length distribution becomes more complex, developing fat tails, indicating correlations at larger length scales. Note that even with the existence of shear, the deviation from the exponential distribution is minor, i.e., only for the rare events at the tail part. The insets of Fig. 3 plot the histograms of a single realization, where the exponential distribution provides reasonable fit to the data points.

To see how the results presented above depend on the parameters δ and α, we have performed the similar analysis for different values of δ and α. Figure 3 shows that when α and δ vary, the distributions change slightly. The dependence of λ, Δ, and β on δ and α can be obtained quantitatively. In Fig. 3(a), λ, Δ, and β are respectively 1.31, 1.23, and 0.85 for

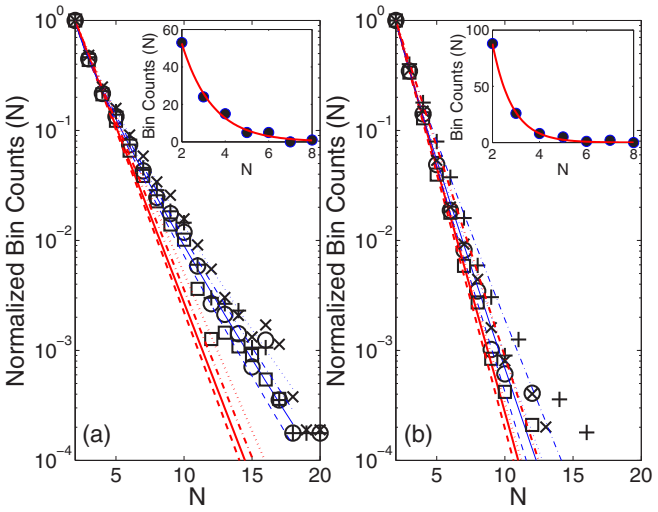

FIG. 3. (Color online) Histograms of force-chain length distributions in (a) pure shear and (b) isotropic compression. In main panels of (a) and (b), different symbols represent different values of α and δ, with $\alpha = 0.25$ and $\delta = 20^\circ$ (circles), $\alpha = 0.2$ and $\delta = 20^\circ$ (squares), $\alpha = 0.25$ and $\delta = 25^\circ$ (crosses), and $\alpha = 0.25$ and $\delta = 20^\circ$ (pluses). Red thick (respectively, blue thin) lines are the exponential (respectively, stretched exponential) fits, with $\alpha = 0.25$ and $\delta = 20^\circ$ (solid lines), $\alpha = 0.2$ and $\delta = 20^\circ$ (dashed lines), $\alpha = 0.25$ and $\delta = 25^\circ$ (dotted lines), and $\alpha = 0.25$ and $\delta = 20^\circ$ (dash-dotted lines). The results in main panel (a) [respectively, in main panel (b)] are produced from a subensemble of 103 (respectively, 67) realizations at $Z = 3.93 \pm 0.04$ (respectively, at $Z = 4.22 \pm 0.04$). Distributions of a single realization are shown in the insets of panels (a) and (b) for $\alpha = 0.25$ and $\delta = 20^\circ$ with solid lines from the exponential fit. For easy comparison, the bin counts in each data set of the two main panels are normalized by the counts in its first bin accordingly.

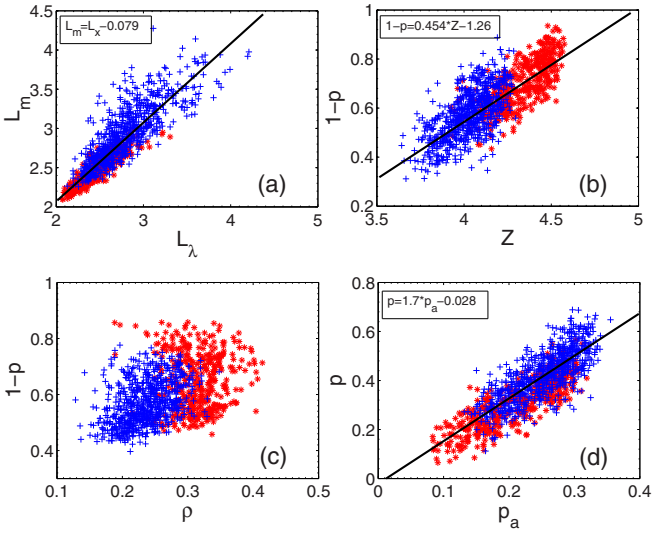

FIG. 4. (Color online) Scatter plot of (a) mean force-chain length obtained using Eq. (1) in the main text, L_λ, versus the directly measured value L_m. (b) Mean contact number Z versus $(1 - p)$. (c) Density of chain branching particles ρ versus $(1 - p)$. (d) p_a versus p. Solid lines show the linear fit. Each data point is from a single realization of an experiment of either pure shear (blue plus signs) or isotropic compression (red stars). Here $\alpha = 0.25$ and $\delta = 20^\circ$.

$\alpha = 0.2$ and $\delta = 20^\circ$; 1.52, 1.42, and 0.84 for $\alpha = 0.25$ and $\delta = 25^\circ$; and 1.42, 1.33, and 0.84 for $\alpha = 0.3$ and $\delta = 20^\circ$. Similarly in Fig. 3(b), λ, Δ, and β are respectively 0.94, 0.92, and 0.95 for $\alpha = 0.2$ and $\delta = 20^\circ$; and 1.0, 0.97, and 0.92 for $\alpha = 0.3$ and $\delta = 20^\circ$. Extensive analysis has been performed for data at other Z (data not shown here in Fig. 3). At a given Z, the exponent β remains nearly constant, showing a weak dependence on the parameters δ and α and hence preserving the shape of distributions. For different values of Z, the exponent β shows small variations with values in the range of $0.9 \sim 1.0$ in isotropic compression, slightly larger compared to the pure shear, which has values in the range of $0.8 \sim 0.9$. When δ is fixed, as α increases from 0.15 to 0.3, λ and Δ increase from a few percent up to twenty percent, depending on the value of δ. When α is larger than 0.3, two parallel neighboring chains cannot be distinguished anymore. When α is fixed, as δ increases from 15° to 25°, λ and Δ increase from ten percent up to twenty percent, depending on the value of α. $\alpha = 0$ corresponds to perfectly aligned chains, which is unrealistic in practical applications. The average alignment angle between neighboring particles is around 20° in pure shear and 25° in isotropic compression. Hence we typically choose δ around $20^\circ \sim 25^\circ$ as a natural and optimal value.

To gain some insight, we approximate force-chain length distribution with an exponential distribution to focus on the isotropic part of the force network by ignoring the deviation from an exponential distribution. To make progress, we first assume that the probability of a particle being part of a force chain is a constant p. It is easy to find that the probability $P(N)$ of a length of an N-particle force chain is $P(N) = p^N(1 - p)$. Hence $\ln(P(N)) = \ln(p)N + \ln(1 - p)$. Defining $\ln(p) \equiv -\frac{1}{\lambda}$ or equivalently $p = e^{-1/\lambda}$ yields $P(N) \propto e^{-N/\lambda}$, which is the discrete exponential distribution with only one free parameter λ. For an arbitrary distribution $P(N)$ of the force-chain length N, the mean force-chain length L_m can be computed by using

$$L_m \equiv \frac{\sum N P(N)}{\sum P(N)} \tag{1}$$

by definition. When $P(N) = p^N(1 - p)$, L_m can be calculated analytically using

$$L_m = 2 + p/(1 - p). \tag{2}$$

Because $p = e^{-1/\lambda}$ and experimentally it is straightforward to find λ through the exponential fit of the distribution $P(N)$, therefore once λ is found, p can be determined, and L_m can then be computed using the above Eq. (2). We define

$$L_\lambda \equiv 2 + e^{-1/\lambda}/(1 - e^{-1/\lambda}) \tag{3}$$

to emphasize that this average chain length is obtained through the exponential fit. In contrast, we compute L_m directly using Eq. (1). Note that L_m and L_λ are the same only when $P(N)$ is an exponential distribution.

To check its validity, we show the scatter plot of L_λ versus L_m in Fig. 4(a). Note that each data point in Fig. 4 is a single realization, i.e., the statistics of a single image similar to the insets of Fig. 3. Despite the fluctuation, the linear fit indicates that an exponential distribution provides

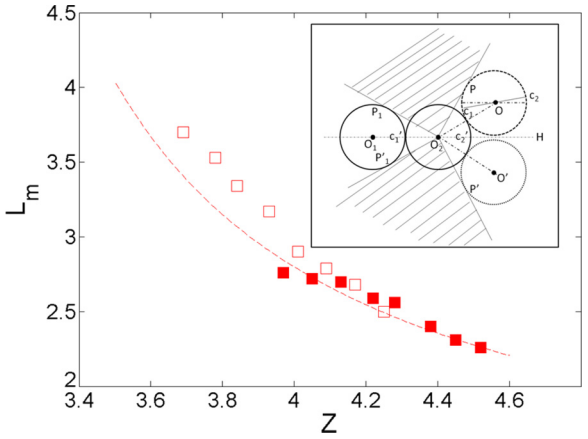

FIG. 5. (Color online) The mean length scale L_m of force-chain length distributions as a function of the average contact number Z measured from isotropic compression (red solid squares) and pure shear (red open squares) at $\alpha = 0.25$ and $\delta = 20^\circ$. The dashed line is the prediction of Eq. (5) in the main text. The inset is a schematic for an estimation of Z^* in Eq. (4) in the main text based on geometry. Each data point is computed from a subensemble of realizations at a given Z. We note that the original ensembles of isotropic compression and pure shear have been divided into eight subensembles according to the average contact number Z. Each data point in the above figure is a result of an individual subensemble.

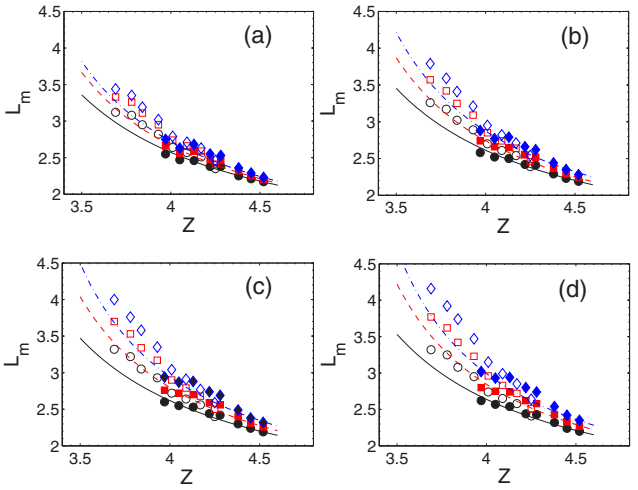

FIG. 6. (Color online) The mean force-chain length L_m versus the average contact number Z measured in isotropic compression (solid symbols) and pure shear (open symbols). Different panels (a–d) have different values of α with $\alpha = 0.15$ in (a), $\alpha = 0.2$ in (b), $\alpha = 0.25$ in (c), and $\alpha = 0.3$ in (d). In each panel, results of different values of δ are plotted using different symbols: $\delta = 15^\circ$ (circles), $\delta = 20^\circ$ (squares), and $\delta = 25^\circ$ (diamonds). The lines are fitting using equation (3) with different line styles for different δ: $\delta = 15^\circ$ (solid lines), $\delta = 20^\circ$ (dashed lines), and $\delta = 25^\circ$ (dash-dotted lines).

a good estimate of the mean chain length. A key question is what determines p, or equivalently $1 - p$. In principle, p depends not only on the local geometry but also on the mechanical properties of the local force network, which are in general quite complex in nature. To make progress, we make a mean-field approximation assuming that $1 - p$ is only related to the average number of contacts per particle Z. A linear fit in Fig. 4(b) yields

$$(1 - p) = aZ - b \propto Z - Z^*, \tag{4}$$

with $a = 0.454$, $b = 1.26$, and $Z^* = 2.78$. Using the inset of Fig. 5, we can give a rough estimate of Z^* based on geometry. For simplicity, monodisperse disks are drawn and the stress orientation of the disk O_2 is horizontal. Here the disks O_1 and O_2 belong to the same force chain and the disk O and its mirror image O' are at the marginal positions of the force chain. Hence $1 - p$ is proportional to the azimuthal angle of the shaded area. Assuming a uniform distribution of contacts, Eq. (4) implies that Z^* is the number of contacts proportional to the azimuthal angle Ω, of the nonshaded area. In the inset of Fig. 5, angles $P_1O_2O_1$, $P_1'O_2O_1$, PO_2O, and $P'O_2O'$ are 30° and the stress orientation c_1c_2 of disk O is tilted at a 20° angle compared with the disk O_2. The angle OO_2H is determined by setting the ratio between the area of the polygon $c_1c_2c_2'c_1'$ and total area of the disks O and O_2 equal to $\alpha = 0.25$. Here c_1' and c_2' are the crossing points between O_1H and the circumference of the disk O_2. The angle OO_2H thus equals 33.5°, implying $\Omega = 187^\circ$. We estimate $Z^* = 2.13$ using $Z^* = Z_a\Omega/360^\circ$ with an *adhoc* median value $Z_a = 4.1$ on the horizontal axis of Fig. 5. This Z^* is smaller than, although close to, the above fit value, indicating the correlation of contact distributions between neighboring particles. We note that, in pure shear, Z_a could be smaller, but because contacts are distributed nonuniformly, e.g., along the O_1O_2 direction, an effective Z^* will be bigger. Combining Eqs. (2) and (4) yields

$$L_m = 2 + \frac{1 + b - aZ}{aZ - b}. \tag{5}$$

In principle, $1 - p$ also depends on the density of branching particles ρ of the force network. However, it is a weak effect, as shown in Fig. 4(c). In Fig. 4(b), p is measured using $p = e^{-1/\lambda}$. Experimentally, we also measure the fraction of particles of all identified force chains p_a. Both p and p_a reflect the characteristics of the force-chain network. We expect that p and p_a shall be related. Fig. 4(d) confirms that p_a is on average proportional to p with $p = 1.7p_a$.

In Fig. 5 we compare experimental data points with equation (5) when $\alpha = 0.25$ and $\delta = 20^\circ$, showing a good agreement. It should be noted that in Fig. 5 L_m of each data point is computed using Eq. (1) for a set of realizations of a given contact number Z. To see the dependence of the above results on α and δ, in Fig. 6 we plot experimentally measured values of L_m versus Z along with the mean-field curves of Eq. (5) for various combinations of α and δ. For different sets of parameters α and δ, the results are consistent with what have been observed in the main panel of Fig. 5. The mean-field model shows a reasonably good agreement with the actual values of L_m within the experimental range of Z, with better agreement in isotropic compression than in pure shear. The maximum deviation of the predicted value of L_m compared to the actual value is off by ~10% as displayed in Fig. 7.

Equation (5) is surprising, considering that Z is a local property, independent of the system size $N_{\rm sys}$, whereas L_m may depend on $N_{\rm sys}$. Intuitively, as $N_{\rm sys}$ increases, one might find

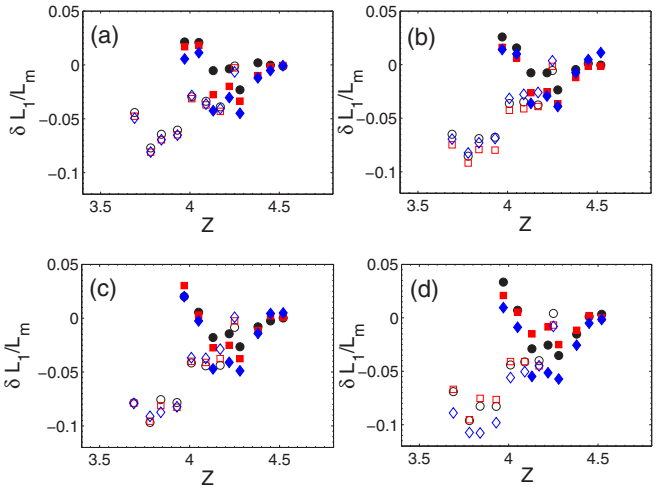

FIG. 7. (Color online) The ratio $\delta L_1/L_m$ versus the average contact number Z in isotropic compression (solid symbols) and pure shear (open symbols). Here δL_1 is the difference between the prediction of Eq. (5) and the actual measurement L_m in Fig. 6. Different panels (a)–(d) have different values of α with (a) $\alpha = 0.15$, (b) $\alpha = 0.2$, (c) $\alpha = 0.25$, and $\alpha = 0.3$ in (d). In each panel, results of different δ are plotted using different symbols: $\delta = 15^\circ$ (circles), $\delta = 20^\circ$ (squares), and $\delta = 25^\circ$ (diamonds).

longer force chains, causing L_m to increase. In Fig. 8 we plot L_m versus $N_{\rm sys}$, with results obtained by analyzing force-chain statistics in small portions of the system of various sizes $N_{\rm sys}$ in the number of particles. In Fig. 8, starting from $N_{\rm sys} = 33$, L_m increases rapidly, and as $N_{\rm sys} > 400$, L_m starts to reach a plateau, independent of the system size. Intuitively, if $N_{\rm sys}$ is

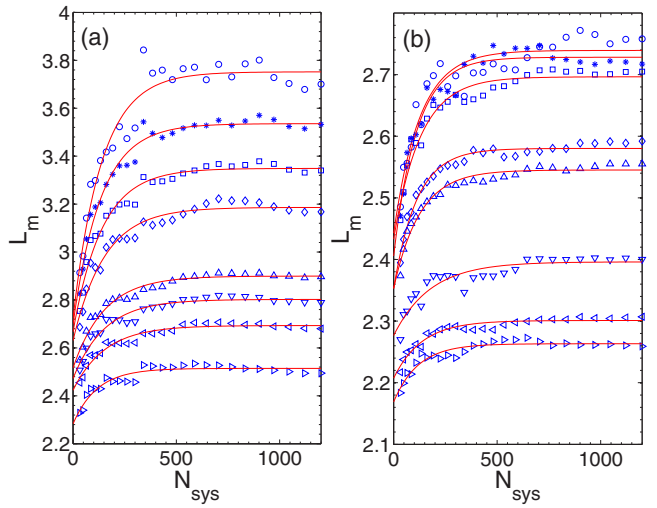

FIG. 8. (Color online) The mean length scale L_m of force-chain length distributions as a function of system size $N_{\rm sys}$ (a) in pure shear at different contact number Zs of 3.67 (○), 3.78 (∗), 3.85 (□), 3.93 (◇), 4.01 (△), 4.09 (▽), 4.17 (◁), and 4.24 (▷), and (b) in isotropic compression at different Zs of 3.97 (○), 4.05 (∗), 4.13 (□), 4.22 (◇), 4.29 (△), 4.37 (▽), 4.44 (◁), and 4.52 (▷). The solid lines are guides to the eye, obtained from the fit of $L_m = c_1 - c_2 e^{-N_{\rm sys}/c_3}$. Here results are obtained at $\alpha = 0.25$ and $\delta = 20^\circ$; results at other values of α and δ are similar.

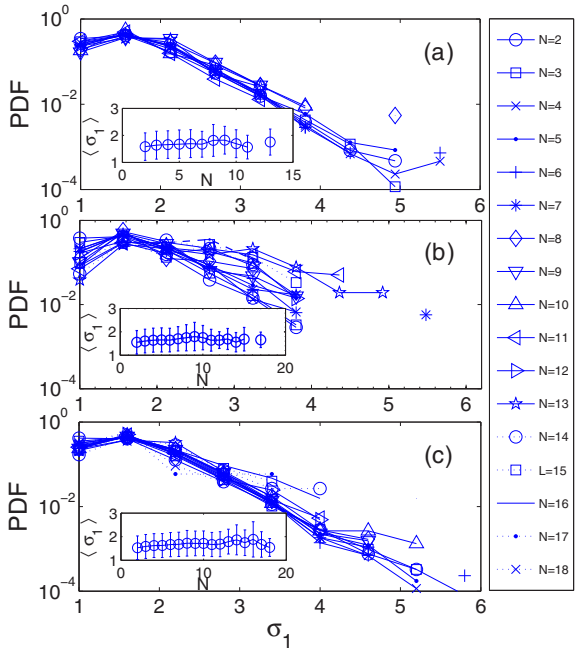

FIG. 9. (Color online) The main panels of (a) with $\alpha = 0.15$, $\delta = 15^\circ$, (b) with $\alpha = 0.25$, $\delta = 20^\circ$, and (c) with $\alpha = 0.3$, $\delta = 25^\circ$ plot the PDFs of σ_1 of chains of different lengths L. The insets of each panel show the conditional average of σ_1 versus the chain length. The average is computed over different groups of force-chain particles according to the chain length. Error bars are estimated from the standard deviation. Here $Z = 4.0$; results from other Z are similar. For simplicity, only results from pure shear are presented; results from isotropic compression are similar.

too small, the finite size effect becomes important; when it is sufficiently large, a further increase in $N_{\rm sys}$ will lead to longer force chains but a simultaneous existence of more shorter force chains. For instance, in Fig. 3, a larger system size implies that more tail part of the distributions will be discovered and a simple calculation can show that the contribution for N going beyond the present limit to infinity contributes less than 0.1% to L_m.

The stress distribution in a granular system typically shows an exponential-like long tail, which can be understood from a Boltzmann-type argument [21,22]. One possible explanation of the above results is that it is directly related to the stress distribution. To check this, we measured the stress distribution of chains of different lengths; three sets of typical results are shown in Fig. 9 for different pairs of α and δ, where the conditional average of the particle stress magnitude is almost independent of the force-chain length. In addition, the distributions all show qualitatively the same behavior. Hence we find no convincing evidence that there is a direct connection between the distributions of force-chain lengths and stresses. In Fig. 9, we only plotted results for three sets of parameters $\alpha = 0.15$, $\delta = 15^\circ$; $\alpha = 0.2$, $\delta = 20^\circ$; and $\alpha = 0.3$, $\delta = 25^\circ$ at Z = 4.0. Results from other values of α, δ, and Z are qualitatively the same. These results have confirmed that the existence of a weak correlation between stress distributions and force-chain length distributions, i.e., particles of longer force chains do not necessarily carry larger stresses.

IV. CONCLUSIONS

In summary, we presented detailed experimental measurements of force-chain length distributions for pure shear and isotropic compression. The distribution shows a slight change from an exponential decay to a stretched exponential decay at the tail part as the shear is applied, consistent with the anisotropic nature of the force-chain network. We understood the isotropic nature of the force-chain length distribution by using a random-walk-type argument and constructed a simple mean-field model to establish a quantitative relation between the average contact number Z of each individual particle and the average force-chain length scale L_m. The model and the experimental results are in a reasonably good agreement. A careful examination shows that L_ms are already at the large system size limit in the present system. Next, we checked the possible connection between the force-chain length distribution and the stress magnitude distribution and found no evidence that these two are directly connected. These results have been checked to be robust, independent of the particular values of the two parameter defined in the force-chain identification algorithm.

ACKNOWLEDGMENTS

J.Z. warmly thanks the hospitality of Professor Bob Behringer's group, where the experiments were performed and support through the startup fund of SJTU, the award of the Chinese 1000-plan(C) fellowship, and Shanghai Pujiang Program (13PJ1405300). Discussions with Dr. Bob Ecke and Dr. Bob Behringer during the DFD 2012 meeting in San Diego are greatly appreciated.

[1] H. M. Jaeger, S. R. Nagel, and R. P. Behringer, Rev. Mod. Phys. **68**, 1259 (1996).
[2] J. Duran, *Sands, Powders, and Grains: An Introduction to the Physics of Granular Materials (Partially Ordered Systems)* (Springer, New York, 1999).
[3] C. h. Liu, S. R. Nagel, D. A. Schecter, S. N. Coppersmith, S. Majumdar, O. Narayan, and T. A. Witten, Science **269**, 513 (1995).
[4] P. Dantu, Geotechnique **18**, 50 (1968).
[5] J. Geng, D. Howell, E. Longhi, R. P. Behringer, G. Reydellet, L. Vanel, E. Clément, and S. Luding, Phys. Rev. Lett. **87**, 035506 (2001).
[6] T. S. Majmudar and R. P. Behringer, Nature (London) **435**, 1079 (2005).
[7] A. J. Liu and S. R. Nagel, Nature (London) **396**, 21 (1998).
[8] M. van Hecke, J. Phys.: Condens. Matter **22**, 033101 (2010).
[9] D. Bi, J. Zhang, B. Chakraborty, and R. P. Behringer, Nature (London) **480**, 355 (2011).
[10] K. To, P.-Y. Lai, and H. K. Pak, Phys. Rev. Lett. **86**, 71 (2001).
[11] F. Radjai, D. E. Wolf, M. Jean, and J.-J. Moreau, Phys. Rev. Lett. **80**, 61 (1998).
[12] M. Sperl, Granular Matter **8**, 59 (2006).
[13] X. Jia, C. Caroli, and B. Velicky, Phys. Rev. Lett. **82**, 1863 (1999).
[14] D. S. Bassett, E. T. Owens, K. E. Daniels, and M. A. Porter, Phys. Rev. E **86**, 041306 (2012).
[15] P. A. Johnson and X. Jia, Nature (London) **437**, 871 (2005).
[16] J. F. Peters, M. Muthuswamy, J. Wibowo, and A. Tordesillas, Phys. Rev. E **72**, 041307 (2005).
[17] L. Sanfratello, J. Zhang, S. Cartee, and E. Fukushima, Granular Matter **13**, 511 (2011).
[18] F. Radjai, M. Jean, J.-J. Moreau, and S. Roux, Phys. Rev. Lett. **77**, 274 (1996).
[19] J. H. Snoeijer, T. J. H. Vlugt, W. G. Ellenbroek, M. van Hecke, and J. M. J. van Leeuwen, Phys. Rev. E **70**, 061306 (2004).
[20] E. I. Corwin, H. M. Jaeger, and S. R. Nagel, Nature (London) **435**, 1075 (2005).
[21] S. Henkes and B. Chakraborty, Phys. Rev. E **79**, 061301 (2009).
[22] B. P. Tighe, A. R. T. van Eerd, and T. J. H. Vlugt, Phys. Rev. Lett. **100**, 238001 (2008).
[23] C. Song, P. Wang, and H. A. Makse, Nature (London) **453**, 629 (2008).
[24] M. Clusel, E. I. Corwin, A. O. N. Siemens, and J. Brujić, Nature (London) **460**, 611 (2009).
[25] S. Torquato and F. H. Stillinger, Rev. Mod. Phys. **82**, 2633 (2010).
[26] J. Zhang, T. Majmudar, A. Tordesillas, and R. Behringer, Granular Matter **12**, 159 (2010).